The following Appendix (Appendixes 1-20) is the Electronic Supplementary Material of the article entitled "Half-a-century (1971–2020) of glacier shrinkage and climatic variability in the Bhaga basin, western Himalaya" at https://doi.org/10.1007/s11629-022-7598-9

**Methods used for clean ice mapping: Automatic approach**

For clean ice glaciers mapping, band ratio is a time-efficient and robust method in comparison to manual delineation techniques (Racoviteanu et al. 2008; Racoviteanu et al. 2009; Rastner et al. 2012; Wang et al. 2014; Schmidt and Nüsser 2012; Bhambri et al. 2012; Chand and Sharma 2015). Automated mapping of snow and ice is based on the fact that snow and ice exhibit high reflectance in the visible and near-infrared region (VIS and NIR) compared to the short-wave infrared (SWIR) region of the solar spectrum. Sentinel 2A images for clean ice mapping in the Northern Tibet region using threshold and band ratio techniques were tested (Paul et al. 2016). For the present study following ratios were tested for the Bhaga basin as suggested by Paul et al. (2016).

The following band ratios were tested using Sentinel images:

- (a) the red/SWIR ratio (MSI4/MSI11) using the first SWIR band (MSI11; center wavelength 1.610 µm);
- (b) the red/SWIR ratio (MSI4/MSI12) using the second SWIR band (MSI12; center wavelength 2.19 µm);
- (c) the NIR/SWIR ratio (MSI8/MSI11)

For (a), thresholds are changed in steps of 0.2 (from 1.6 to 3.0). For (b) and (c), thresholds were selected 2.2 and compare with (a). The MSI4/MSI11 ratio performs better than the other two ratios with only minor differences in mapped glacier extents than the MSI8/MSI11 or MSI4/MSI12 ratios (Appendix 5). Band ratio results were smoothed with a median filter (3*3 kernel size) before converting the binary glacier maps to vector files. The SWIR band was resampled from 20 to 10 m using a cubic convolution to calculate the ratios. Water bodies were misclassified as glaciers (Appendix 8), but this is strongly dependent on their turbidity and thus varies from place to place (Paul et al. 2016). It is found that MSI8/MSI11 maps fewer water pixels compared to MSI4/MSI11 and MSI4/MSI12 and is, therefore, less sensitive on turbid lakes. However, none of the band ratios exclude glacier lakes completely. So, manual cross-checking and adjustment of glacier outlines derived using a semi-automatic approach were mandatory almost for every glacier in the Bhaga basin.

The Landsat TM/ETM+ sensors have proven to be a particularly efficient tool for mapping glacier extent and monitoring changes even for small alpine glaciers (Andreassen et al. 2008). However, the major limitation is the availability of suitable cloud-free scenes at the end of the ablation season without remaining seasonal snow. The commonly used band ratio images consider Landsat TM or ETM+ bands 2 (green), 3(red), 4 (NIR), and 5 (SWIR) to take advantage of these spectral differences at different wavelengths and separate clean glacier ice from non-glacier surfaces, for example, band 3/band 5 (Andreassen et al. 2008; Bolch et al. 2010), band 4/band 5 (Paul et al. 2002), and the normalized difference snow index ((band 2 – band 5)/(band 2 + band 5))(Silverio and Jaquet 2005). Clean glacier ice has high values in these ratio images; supraglacial debris and other nearby non-glacier rocky surfaces have low values because the supraglacial debris and the other rocky surfaces have similar spectral responses at these wavelengths.

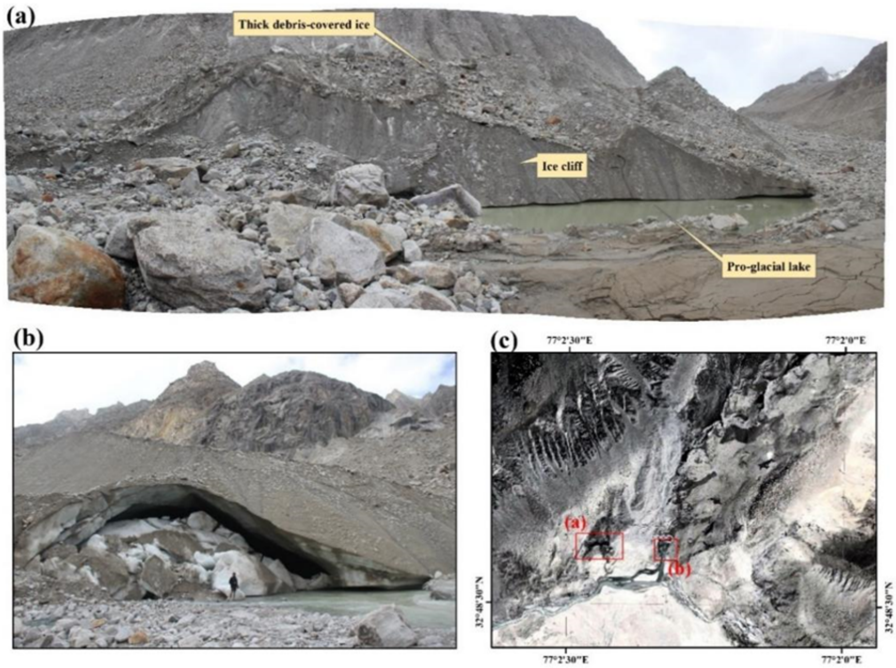


Appendix 1 Terminus characteristics of Dali glacier in 2016. (a) Dead ice part with ponds. (b) Ice collapse. (c) High resolution Google Earth image of terminus zone.

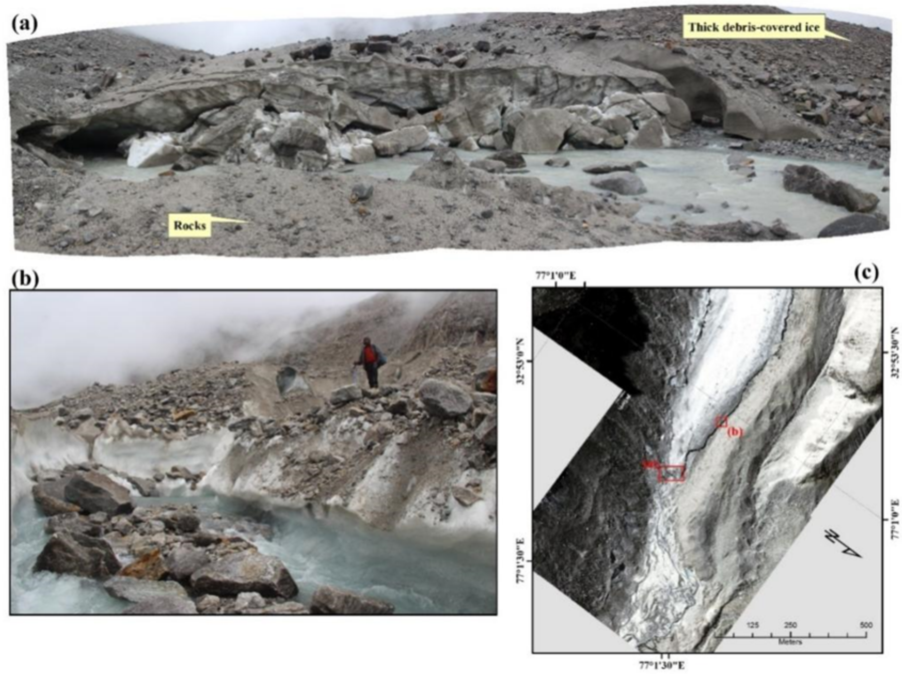


Appendix 2 Terminus characteristics of Mayar I glacier. (a) Snout characteristics. (b) Supraglacial streams. (c) High resolution Google Earth image with location of (a) and (b).

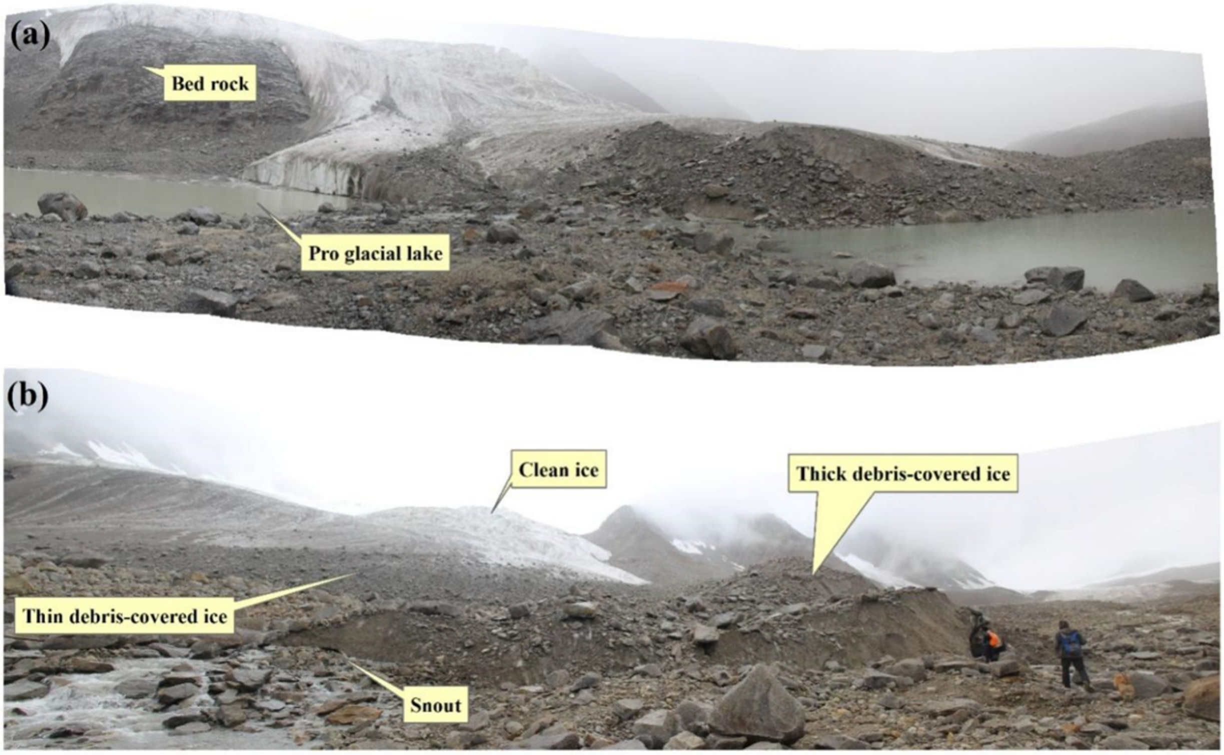


**Appendix 3** Terminus characteristics of Mayar II glacier in 2017.

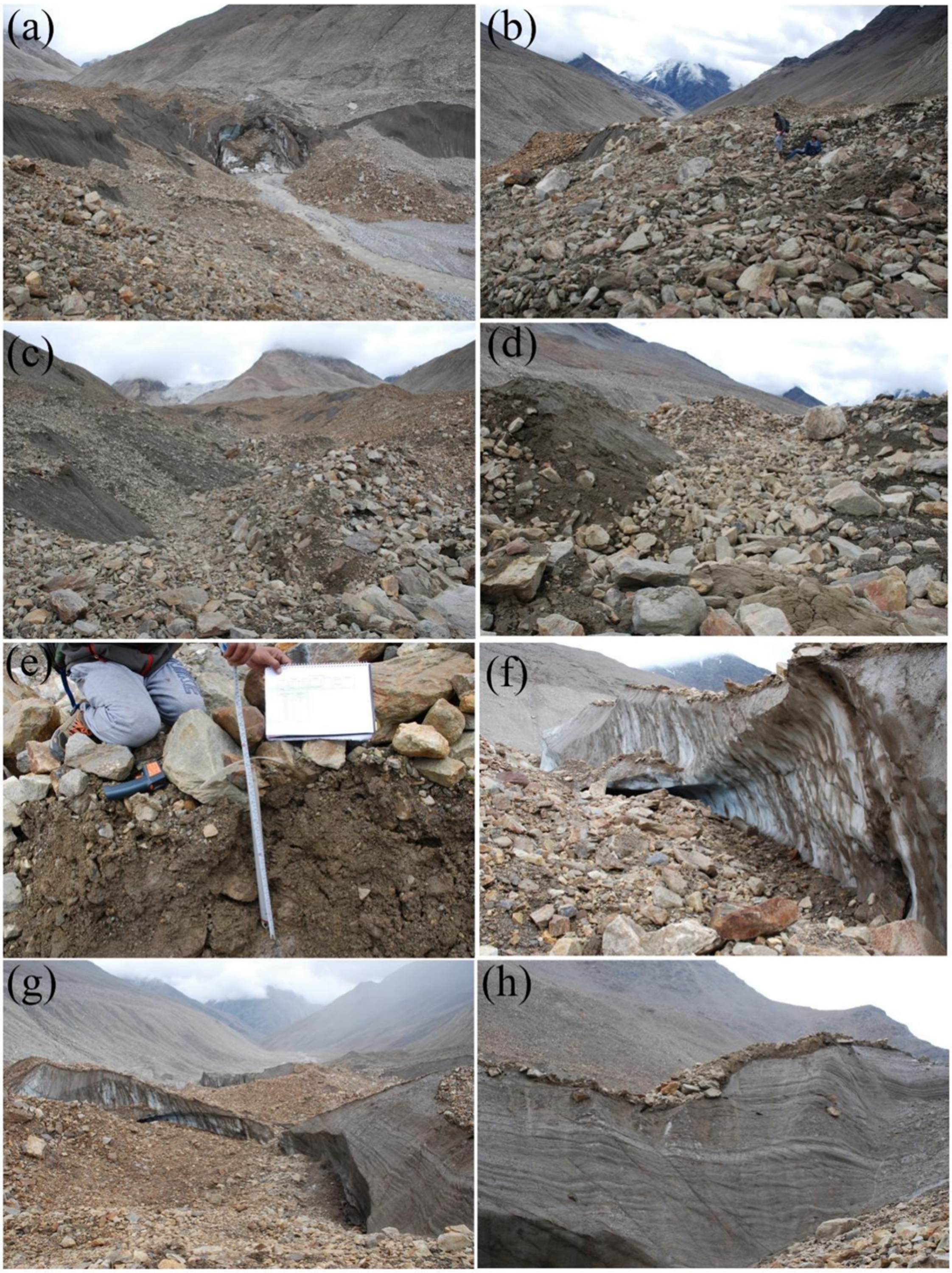


**Appendix 4** Terminus characteristics of the Bagrari Glacier in the Jankar Chhu watershed in 2018. (a) Snout characteristics. (b - d) Debris morphology (shape, size, types). (e) Example of debris thickness measurements. (f – h) Ice cliffs morphology.

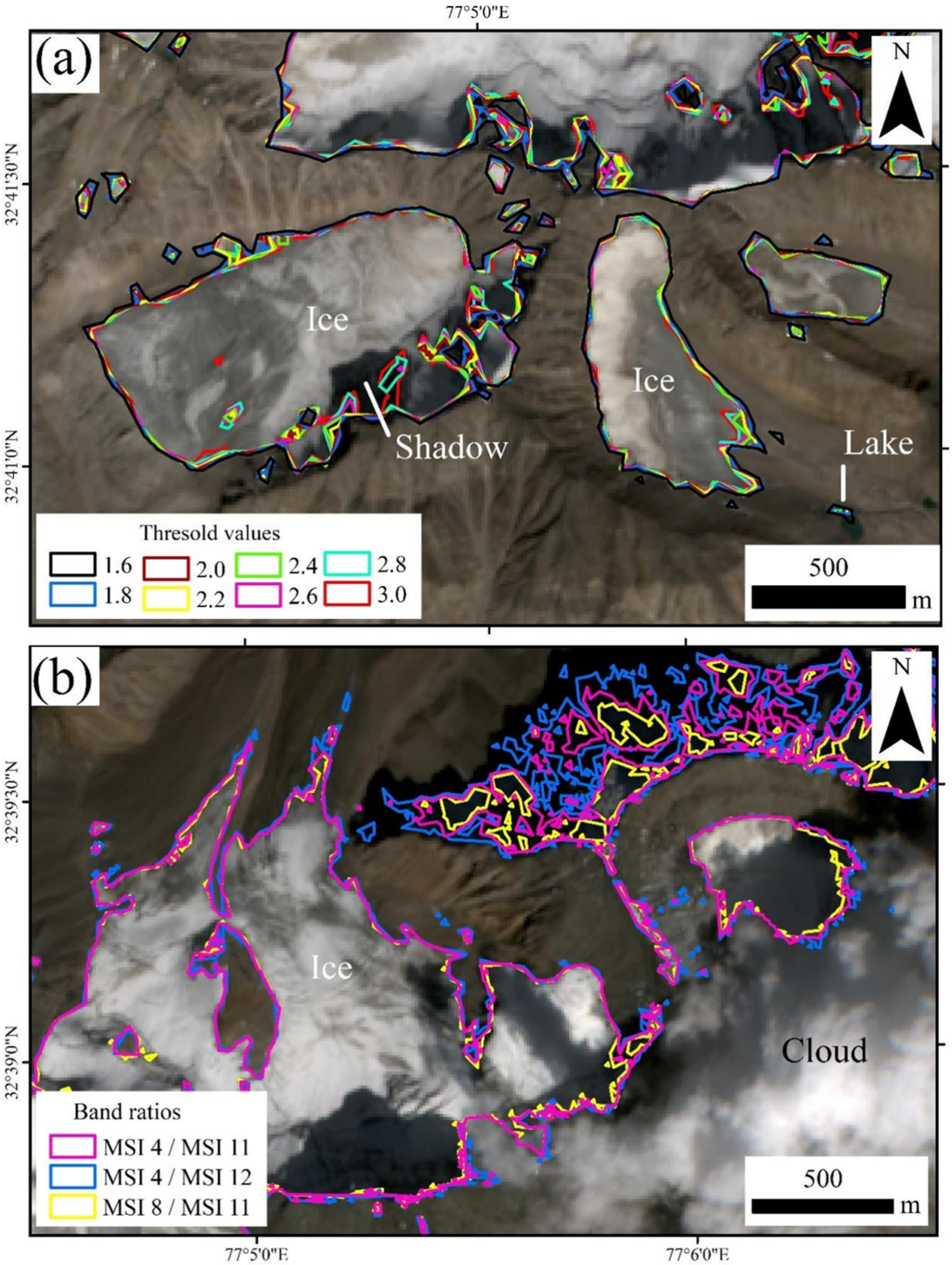


**Appendix 5** Clean ice glaciers mapping using band ratio techniques from Sentinel 2 images. (a) Multiple threshold values were tested using the MSI4/MSI11 bands ratio. Black indicates the largest glacier extent, and red indicates the smallest extent of snow and ice. (b) Three different band ratios were tested using the same thresholds values. Results show misinterpretation of shadow areas, lakes, and cloud cover. Background image FCC with MSI bands 12, 4, and 3 as RGB. Coordinate grid: UTM zone 43N.

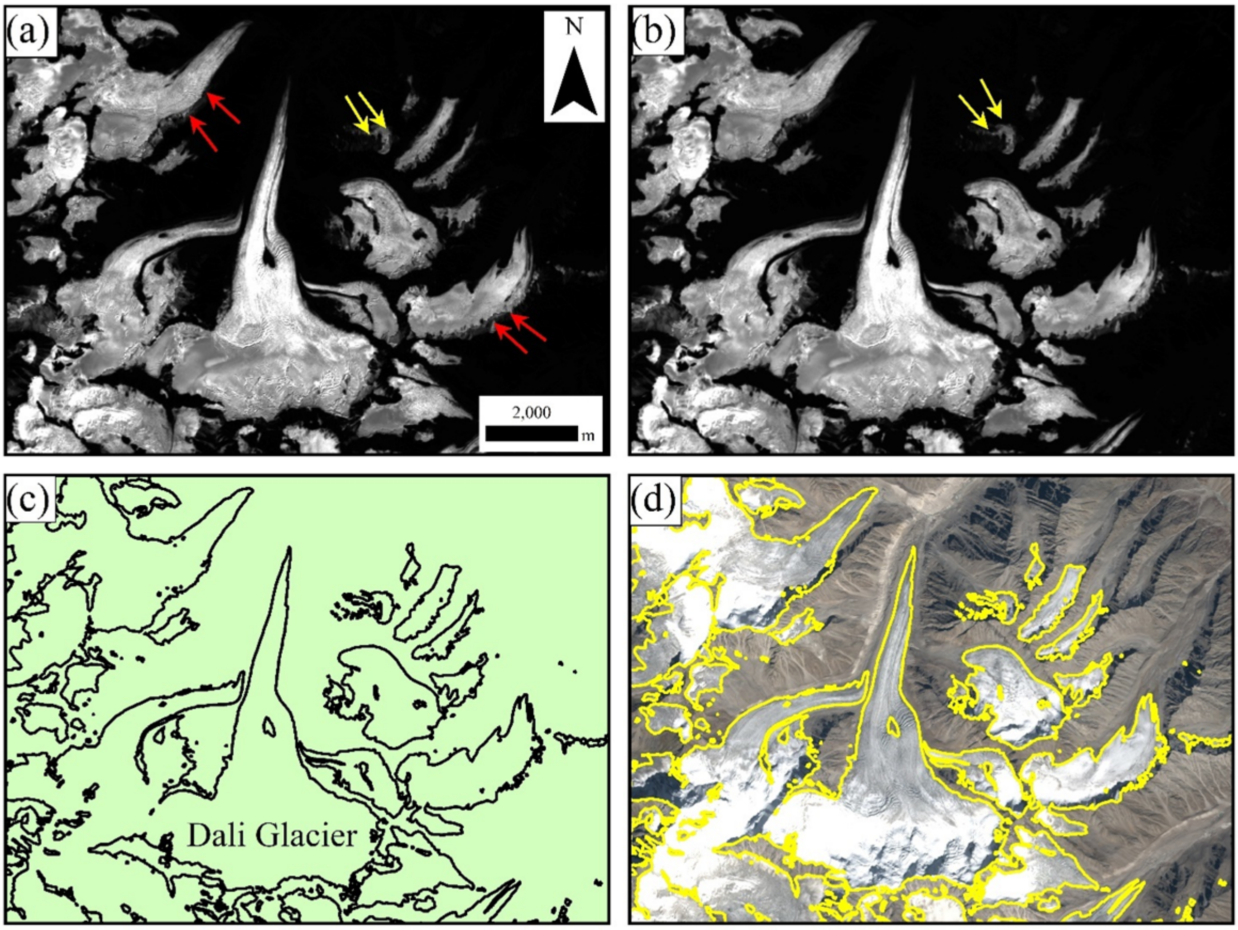


**Appendix 6** Post-processing of band ratio techniques using Sentinel 2A images of 2016. (a) Band ratio (MSI4/MSI11). (b) Effects of kernel 3*3 median filter. (c) Vectorization of glaciers mask using threshold value of 2.1 (d) Clean ice glaciers mask overlaid on Sentinel true color composite. Yellow arrow indicates the effects of median filter. Red arrow indicates shadow area.

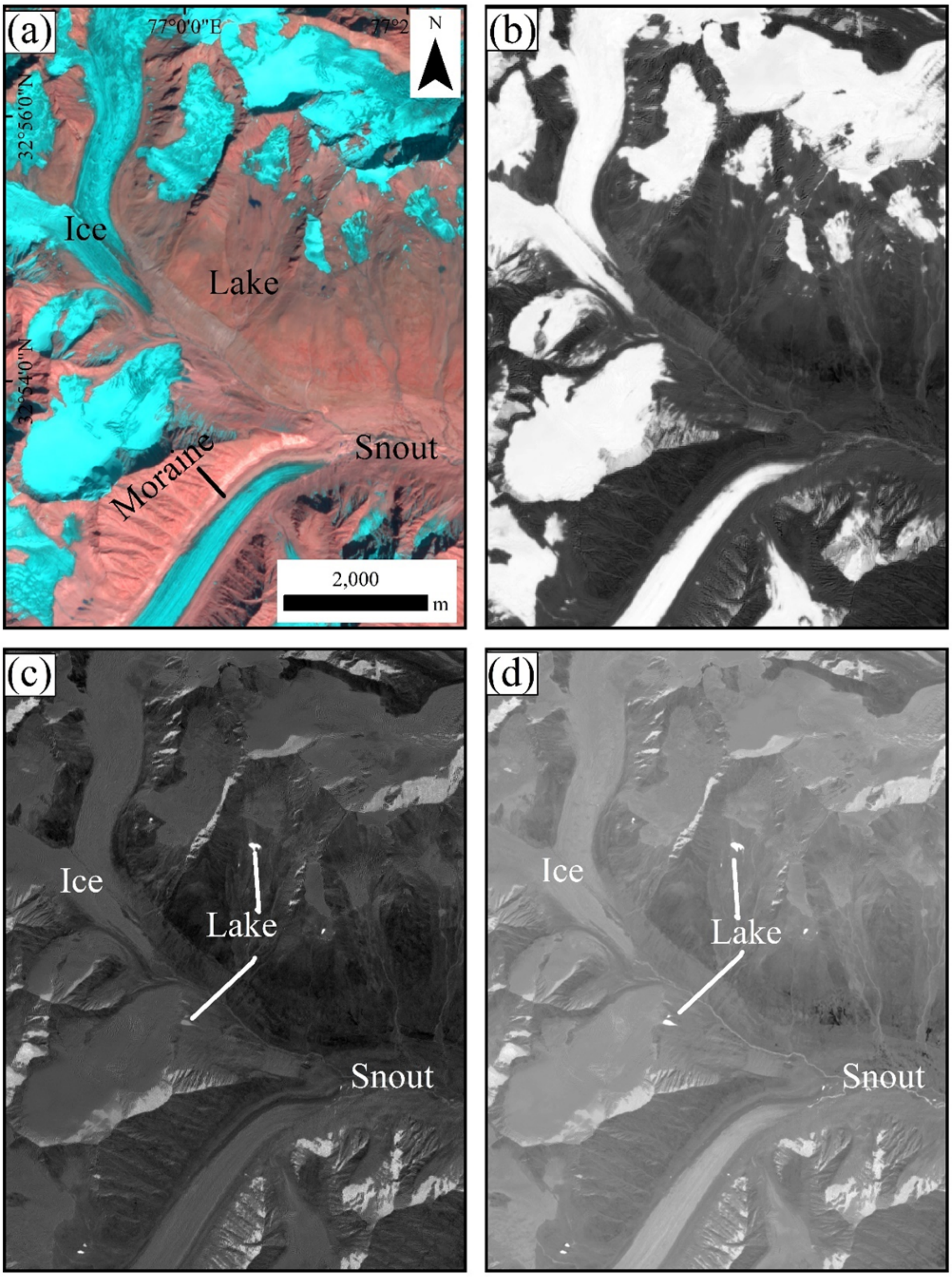


**Appendix 7** Normalized difference indices for clean ice mapping using Sentinel 2A images. Analysis was performed on Sentinel 2A images of 01.11.2016. (a) FCC with MSI bands 12, 4 and 3 as RGB. (b) NDSI (MSI3-MSI11)/ (MSI3+MSI11). (c) NDSII (MSI3-MSI8)/ (MSI3+MSI8). (d) NDGI (MSI3-MSI4)/ (MSI3+MSI4). Clean ice glaciers can be mapped using NDSI but it cannot distinguish between shadow and ice. NDSII and NDGI clearly distinguish water body, although it is difficult to differentiate between shadow and cloud cover areas.

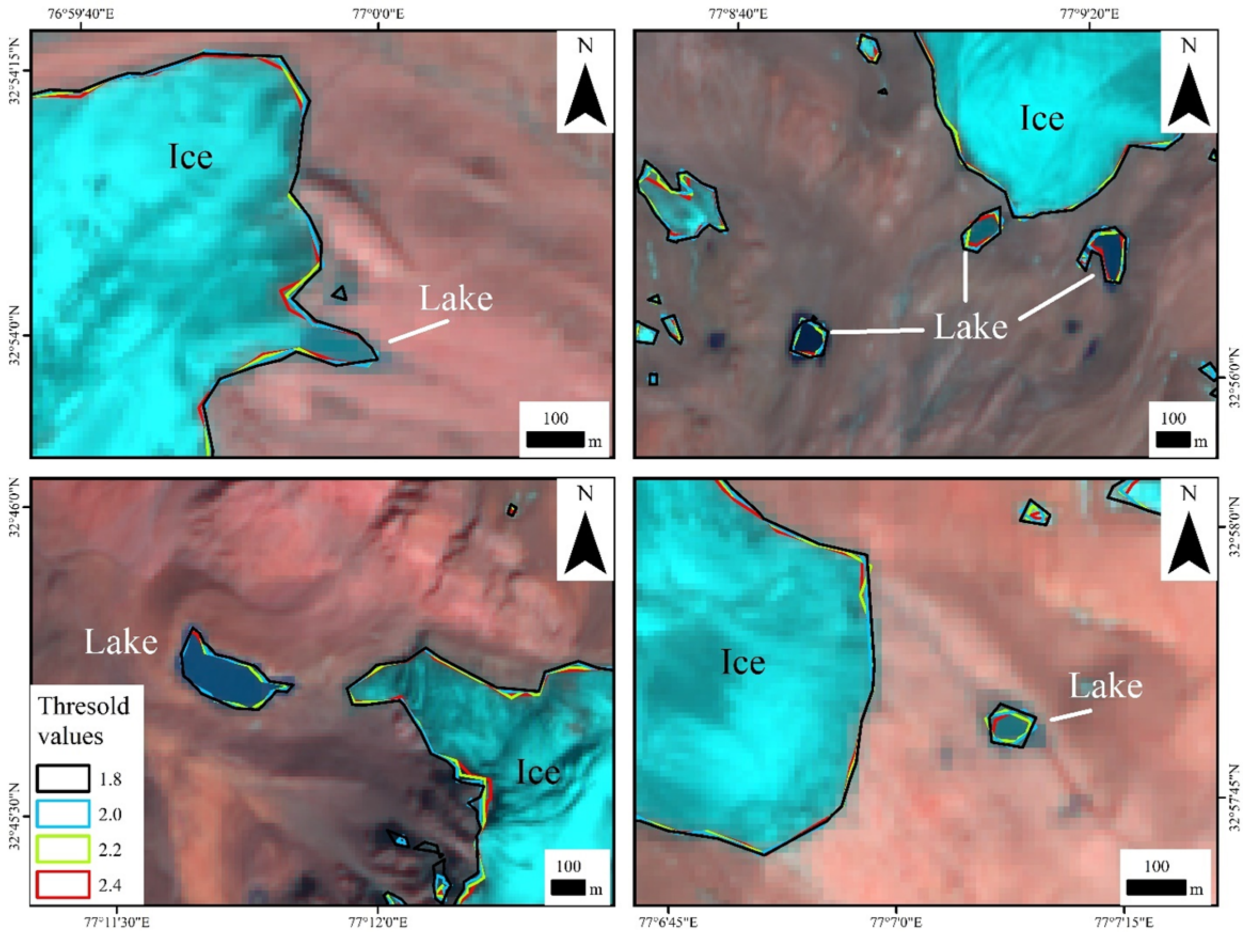


**Appendix 8** Observation of automatic clean-ice glacier mapping from Sentinel 2A images. Automatic clean ice mapping is not effective for differentiating lakes, shadow, and clouds cover areas in the Bhaga basin. Different threshold values were tested although no one gives satisfying results.

**Appendix 9** Glacier mapping uncertainty derived based on buffer method. Details of this method is provided in section 3.5.

| Sensor | Analyzed glaciers | Buffer size (m) | Area with buffer size (km²) | Calculated area (km²) | Uncertainty (km²) | Uncertainty (%) |
|---|---|---|---|---|---|---|
| (a) Uncertainty for mapped 306 glaciers in the Bhaga basin | | | | | | |
| LISS IV | 306 | 2.5 | 364.22 | 360.28 | 3.94 | 1.08 |
| (b) Uncertainty for analyzed 233 glaciers in the Bhaga Basin | | | | | | |
| Corona KH-4B | 233 | 3 | 367.28 | 362.87 | 4.41 | 1.20 |
| Landsat ETM+ | 233 | 7.5 | 357.97 | 347.38 | 10.59 | 2.96 |
| LISS IV | 233 | 2.5 | 340.33 | 336.83 | 3.50 | 1.03 |
| Sentinel 2A | 233 | 5 | 342.35 | 335.38 | 6.97 | 2.04 |
| Sentinel 2B | 233 | 5 | 341.07 | 334.10 | 6.96 | 2.04 |

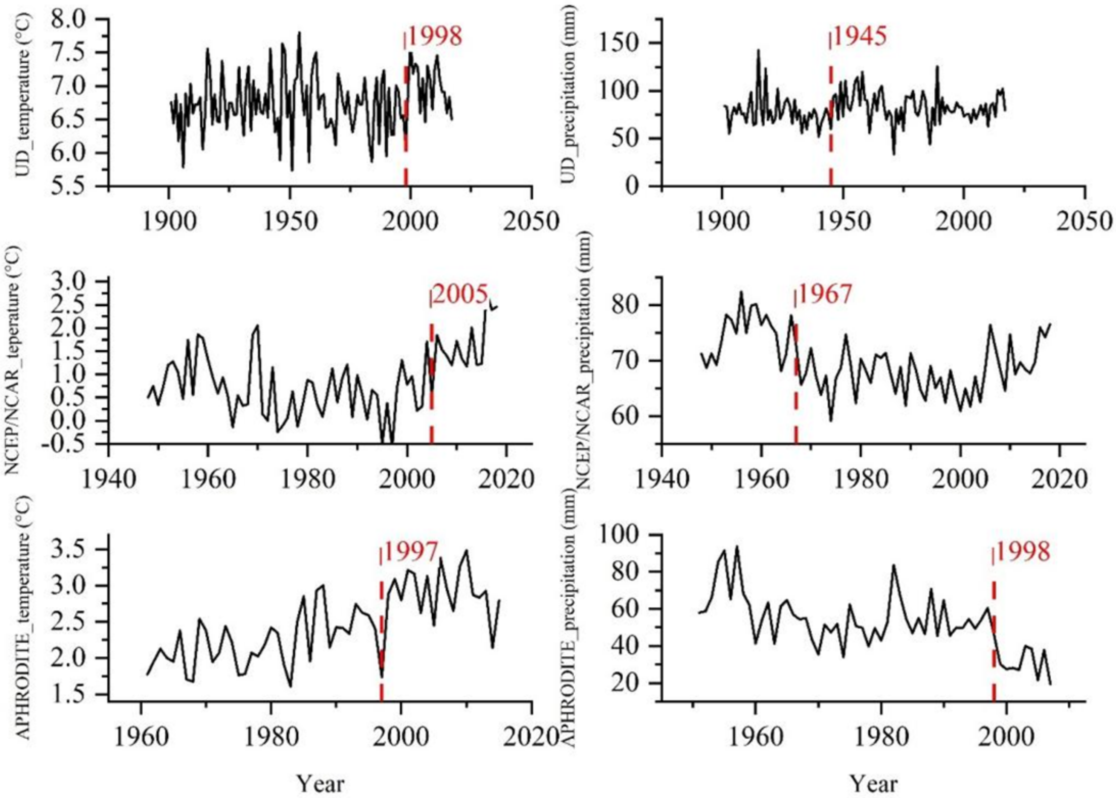


**Appendix 10** Change point analysis for climatic data used in this study. Change point analysis tool was used in Origin pro software for identification of break of points. A significant shift was observed for temperature data around 2000.

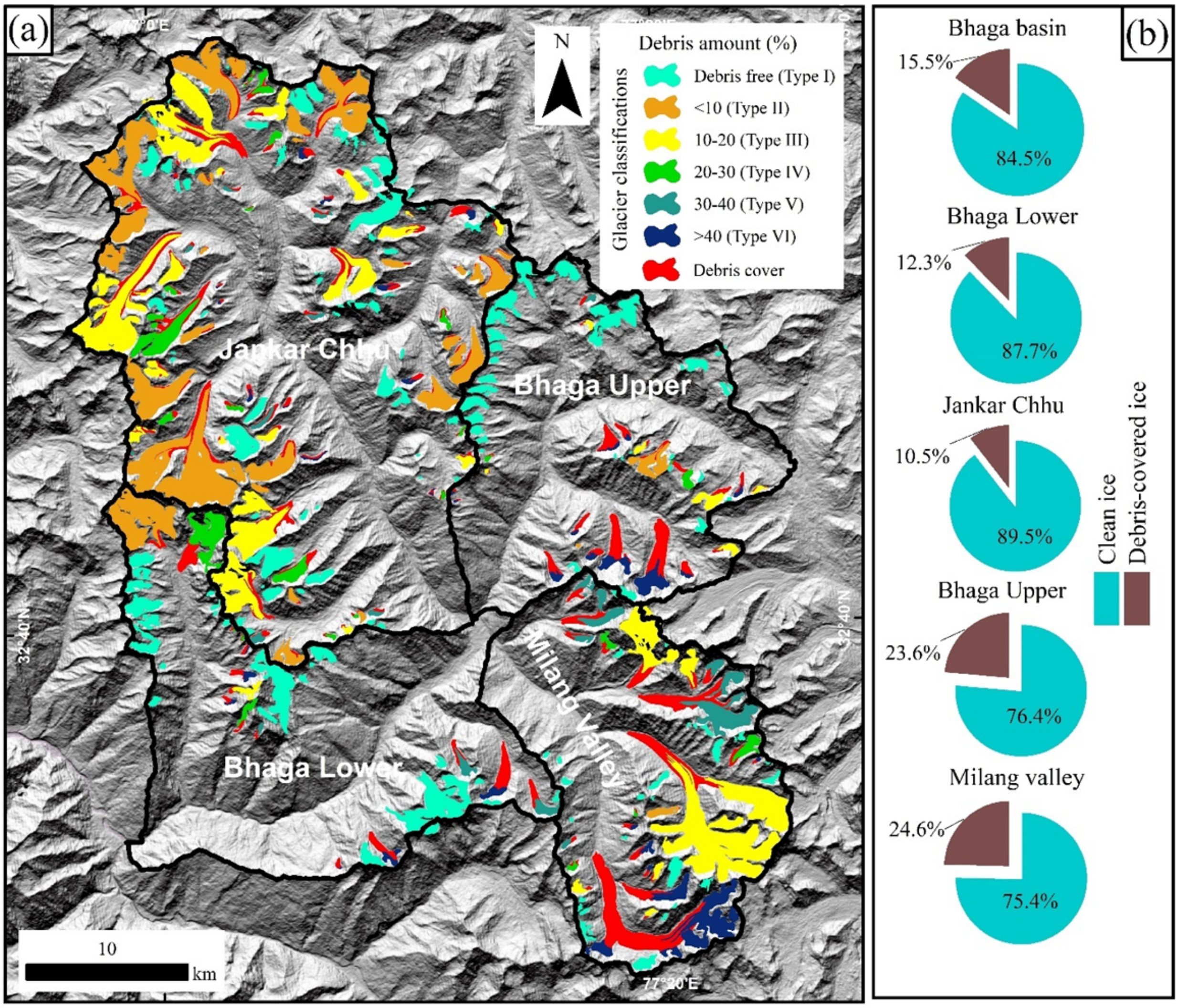


**Appendix 11** Distribution of debris-covered ice in the Bhaga basin and its tributary watersheds in 2013. a) Glaciers were categorized based on their percentage of debris-covered ice. b) Percentage of the debris-covered area to the total area in different watersheds in the Bhaga basin.

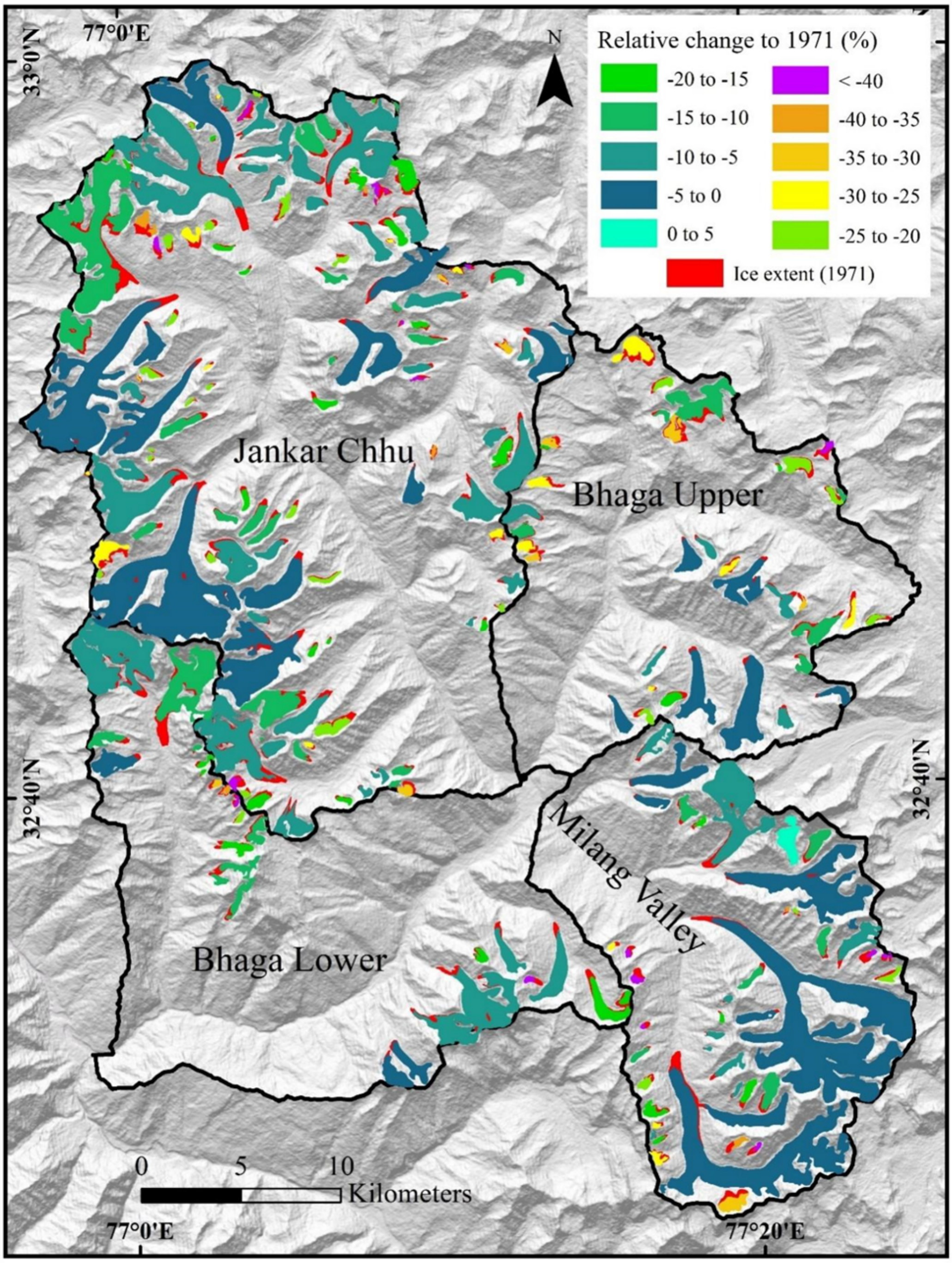


**Appendix 12** Glacier surface area change rate in the Bhaga basin between 1971 and 2020.

**Appendix 13** Multitemporal changes in clean and debris-covered (DC) ice in the Bhaga basin and tributary watersheds during last five decades (1971-2020).

| Years | Ice extent (km²) | | Period | Absolute change (km²) | | Relative change (%) | |
|---|---|---|---|---|---|---|---|
| | Clean ice | DC ice | | Clean ice | DC ice | Clean ice | DC ice |
| (a) Entire Bhaga basin | | | | | | | |
| 1971 | 318.0 ± 3.5 | 44.9 ± 0.5 | 1971-2020 | -42.9 ± 5.0 | 13.9 ± 0.7 | -13.5 ± 1.2 | 31.1 ± 1.6 |
| 2000 | 299.1 ± 3.3 | 48.3 ± 0.5 | 1971-2000 | -18.9 ± 4.7 | 3.4 ± 0.7 | -5.9 ± 0.1 | 7.7 ± 1.4 |
| 2013 | 281.8 ± 3.1 | 54.9 ± 0.6 | 2000-2013 | -17.2 ± 4.2 | 6.7 ± 0.7 | -5.8 ± 0.1 | 13.8 ± 1.5 |
| 2016 | 278.8 ± 3.0 | 56.6 ± 0.6 | 2013-2016 | -3.1 ± 4.2 | 1.6 ± 0.7 | -1.1 ± 0.1 | 2.9 ± 0.1 |
| 2018 | 276.1 ± 3.0 | 58.1 ± 0.6 | 2016-2018 | -2.7 ± 4.2 | 1.4 ± 0.7 | -0.9 ± 0.1 | 2.5 ± 0.1 |
| 2020 | 275.1 ± 3.0 | 58.8 ± 0.6 | 2018-2020 | -1.0 ± 2.1 | 0.7 ± 0.3 | -0.3 ± 0.1 | 1.2 ± 0.1 |
| (b) Bhaga Lower | | | | | | | |
| 1971 | 37.3 ± 0.4 | 6.1 ± 0.1 | 1971-2020 | -4.5 ± 0.5 | 0.1 ± 0.1 | -12.1 ± 1.4 | 1.6 ± 0.1 |
| 2000 | 34.9 ± 0.4 | 6.1 ± 0.1 | 1971-2000 | -2.4 ± 0.5 | -0.1 ± 0.1 | -6.5 ± 1.1 | -0.9 ± 0.1 |
| 2013 | 33.5 ± 0.4 | 5.9 ± 0.1 | 2000-2013 | -1.4 ± 0.5 | 0.1 ± 0.1 | -4.0 ± 0.5 | 2.5 ± 1.2 |
| 2016 | 33.2 ± 0.4 | 6.0 ± 0.1 | 2013-2016 | -0.3 ± 0.5 | -0.03 ± 0.1 | -0.8 ± 0.6 | -0.5 ± 0.8 |
| 2018 | 33.0 ± 0.4 | 6.0 ± 0.1 | 2016-2018 | -0.2 ± 0.5 | 0.02 ± 0.1 | -0.5 ± 0.6 | 0.3 ± 0.8 |
| 2020 | 32.8 ± 0.4 | 6.2 ± 0.1 | 2018-2020 | -0.2 ± 0.5 | 0.2 ± 0.1 | -0.6 ± 0.5 | 3.2 ± 1.2 |
| (c) Jankar Chhu | | | | | | | |
| 1971 | 183.4 ± 2.0 | 12.8 ± 0.1 | 1971-2020 | -23.8 ± 2.6 | 8.4 ± 0.2 | -13.1 ± 2.1 | 65.1 ± 2.4 |
| 2000 | 174.5 ± 1.9 | 14.0 ± 0.2 | 1971-2000 | -8.8 ± 2.6 | 1.2 ± 0.2 | -4.8 ± 1.2 | 9.1 ± 1.3 |
| 2013 | 163.1 ± 1.8 | 19.2 ± 0.2 | 2000-2013 | -11.5 ± 2.6 | 5.2 ± 0.2 | -6.6 ± 1.0 | 36.9 ± 2.1 |
| 2016 | 161.6 ± 1.8 | 19.9 ± 0.2 | 2013-2016 | -1.5 ± 2.6 | 0.7 ± 0.2 | -0.9 ± 1.0 | 3.8 ± 1.2 |
| 2018 | 159.8 ± 1.8 | 20.9 ± 0.2 | 2016-2018 | -1.7 ± 2.6 | 1.0 ± 0.2 | -1.1 ± 1.6 | 4.9 ± 1.3 |
| 2020 | 159.6 ± 1.8 | 21.2 ± 0.2 | 2018-2020 | -0.2 ± 0.1 | 0.3 ± 0.2 | -0.1 ± 0.1 | 1.3 ± 0.5 |
| (d) Bhaga Upper | | | | | | | |
| 1971 | 27.4 ± 0.3 | 6.7 ± 0.1 | 1971-2020 | -6.9 ± 0.3 | 2.3 ± 0.1 | -25.1 ± 2.4 | 34.1 ± 1.2 |
| 2000 | 24.1 ± 0.3 | 7.7 ± 0.1 | 1971-2000 | -3.3 ± 0.3 | 1.0 ± 0.1 | -12.2 ± 2.1 | 14.7 ± 1.2 |
| 2013 | 21.6 ± 0.2 | 8.7 ± 0.1 | 2000-2013 | -2.4 ± 0.3 | 1.0 ± 0.1 | -10.1 ± 2.0 | 12.6 ± 1.2 |
| 2016 | 21.3 ± 0.2 | 8.8 ± 0.1 | 2013-2016 | -0.4 ± 0.3 | 0.1 ± 0.1 | -1.6 ± 1.5 | 1.2 ± 0.5 |
| 2018 | 20.9 ± 0.2 | 8.9 ± 0.1 | 2016-2018 | -0.3 ± 0.3 | 0.1 ± 0.1 | -1.4 ± 1.5 | 1.3 ± 0.5 |
| 2020 | 20.5 ± 0.2 | 9.0 ± 0.1 | 2018-2020 | -0.4 ± 0.1 | 0.1 ± 0.1 | -1.9 ± 1.5 | 1.1 ± 0.4 |
| (e) Milang Valley | | | | | | | |
| 1971 | 69.9 ± 0.8 | 19.2 ± 0.2 | 1971-2020 | -8.8 ± 0.9 | 3.6 ± 0.1 | -12.3 ± 1.5 | 18.7 ± 1.2 |
| 2000 | 65.6 ± 0.7 | 20.4 ± 0.2 | 1971-2000 | -4.3 ± 0.9 | 1.2 ± 0.1 | -6.2 ± 1.0 | 6.4 ± 0.5 |
| 2013 | 63.7 ± 0.7 | 21.1 ± 0.2 | 2000-2013 | -1.9 ± 0.9 | 0.7 ± 0.1 | -2.9 ± 0.9 | 3.4 ± 0.5 |
| 2016 | 62.8 ± 0.7 | 21.9 ± 0.2 | 2013-2016 | -1.0 ± 0.9 | 0.8 ± 0.1 | -1.5 ± 0.9 | 3.7 ± 0.5 |
| 2018 | 62.2 ± 0.7 | 22.3 ± 0.2 | 2016-2018 | -0.5 ± 0.9 | 0.4 ± 0.1 | -0.8 ± 0.5 | 1.6 ± 0.5 |
| 2020 | 61.1 ± 0.7 | 22.8 ± 0.2 | 2018-2020 | -0.1 ± 0.1 | 0.5 ± 0.1 | -0.2 ± 0.1 | 2.1 ± 0.6 |

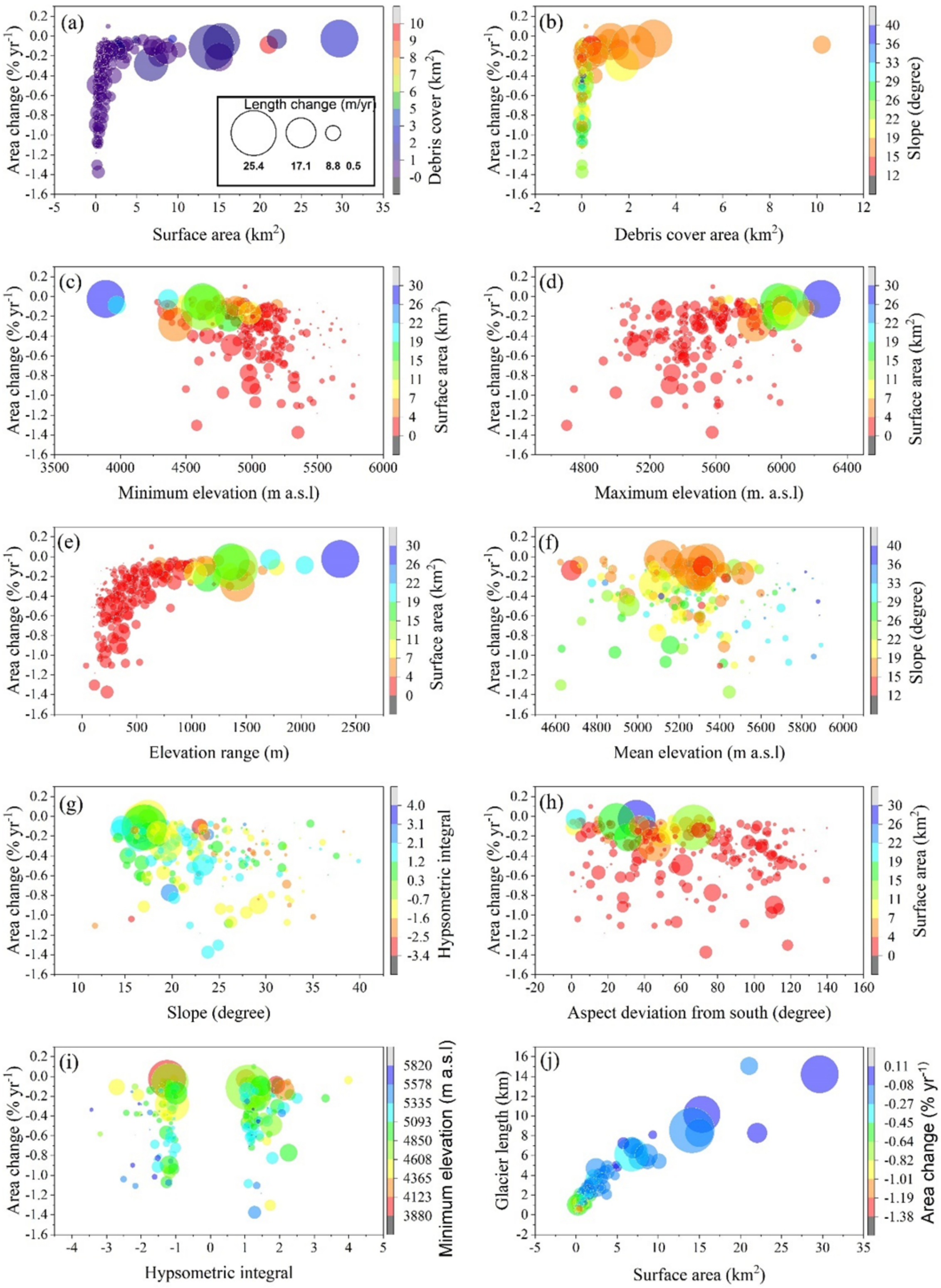


**Appendix 14** Scatter plots between two glacier change indicators (area change and length change) and multiple topographic parameters in the Bhaga basin.

**Appendix 15** Glacier changes in the Bhaga basin based on topographic parameters. *A* = Area, *L* = Length, ASL = Average strip line.

| Parameters | Count | Area change | | | | | Length change | | | | |
|---|---|---|---|---|---|---|---|---|---|---|---|
| | | $A_{1971}$ (km²) | $A_{2020}$ (km²) | Δ*A* (km²) | Δ*A* (%) | Δ*A* (% yr⁻¹) | $L_{1971}$ (m) | $L_{2020}$ (m) | Δ*L* (m) | Δ*L* (m yr⁻¹) | ASL (Δ*L*) (m yr⁻¹) |
| Size class (km²) | | | | | | | | | | | |
| <0.5 | 116 | 25.32 | 18.99 | -6.33 | -25.00 | -0.52 | 758.32 | 609.13 | -149.19 | -3.13 | -3.05 |
| 0.5-1 | 48 | 33.52 | 28.96 | -4.56 | -13.60 | -0.28 | 1619.63 | 1417.97 | -201.66 | -4.22 | -4.25 |
| 1--5 | 52 | 103.72 | 94.86 | -8.86 | -8.54 | -0.18 | 2771.87 | 2504.97 | -266.92 | -5.64 | -5.56 |
| 5--10 | 10 | 73.16 | 68.19 | -4.97 | -6.79 | -0.14 | 6355.07 | 5682.49 | -672.58 | -14.01 | -9.95 |
| >10 | 7 | 127.21 | 122.33 | -4.88 | -3.84 | -0.08 | 10001.3 | 9008.31 | -992.99 | -20.72 | -16.0 |
| Elevation zones (m a.s.l) | | | | | | | | | | | |
| 4600-4800 | 9 | 30.01 | 28.14 | -1.86 | -6.20 | -0.13 | 3485.32 | 3181.30 | -304.02 | -6.33 | -5.74 |
| 4800-5000 | 24 | 17.81 | 15.81 | -2.00 | -11.23 | -0.23 | 1476.45 | 1280.69 | -195.76 | -4.08 | -4.31 |
| 5000-5200 | 51 | 103.55 | 98.01 | -5.54 | -5.35 | -0.11 | 1996.65 | 1746.17 | -250.48 | -5.22 | -4.67 |
| 5200-5400 | 88 | 163.12 | 149.64 | -13.48 | -8.26 | -0.17 | 2221.36 | 1956.03 | -265.33 | -5.53 | -4.95 |
| 5400-5600 | 37 | 44.54 | 39.62 | -4.88 | -10.97 | -0.23 | 1767.53 | 1531.91 | -235.62 | -4.91 | -4.41 |
| 5600-5800 | 17 | 3.07 | 2.31 | -0.76 | -24.76 | -0.52 | 621.20 | 518.23 | -102.97 | -2.15 | -2.07 |
| 5800-6000 | 7 | 0.79 | 0.63 | -0.16 | -20.25 | -0.42 | 478.80 | 399.66 | -79.14 | -1.65 | -1.83 |
| Slope class (degree) | | | | | | | | | | | |
| <15 | 5 | 11.71 | 10.95 | -0.76 | -6.49 | -0.14 | 3117.64 | 2757.77 | -359.87 | -7.50 | -6.92 |
| 15--20 | 77 | 272.37 | 255.51 | -16.86 | -6.19 | -0.13 | 3340.83 | 2986.96 | -353.87 | -7.37 | -6.46 |
| 20-25 | 65 | 51.04 | 44.42 | -6.62 | -12.97 | -0.27 | 1493.25 | 1293.30 | -199.95 | -4.17 | -4.19 |
| 25-30 | 53 | 19.76 | 16.71 | -3.05 | -15.44 | -0.32 | 918.22 | 767.06 | -151.16 | -3.15 | -2.88 |
| >30 | 33 | 7.96 | 6.49 | -1.47 | -18.47 | -0.38 | 752.86 | 619.36 | -133.50 | -2.78 | -2.50 |
| Aspect | | | | | | | | | | | |
| N | 12 | 6.87 | 6.35 | -0.52 | -7.57 | -0.16 | 1228.61 | 1021.34 | -207.27 | -4.32 | -4.83 |
| NE | 57 | 76.56 | 70.1 | -6.46 | -8.44 | -0.18 | 1891.91 | 1661.41 | -230.50 | -4.80 | -4.74 |
| E | 31 | 46.27 | 41.84 | -4.43 | -9.57 | -0.20 | 1714.85 | 1465.11 | -249.74 | -5.20 | -4.65 |
| SE | 16 | 33.51 | 29.24 | -4.27 | -12.74 | -0.27 | 1827.76 | 1497.94 | -329.82 | -6.87 | -5.21 |
| S | 19 | 20.52 | 18.79 | -1.73 | -8.43 | -0.18 | 1418.11 | 1227.40 | -190.71 | -3.97 | -3.54 |
| SW | 13 | 17.41 | 15.53 | -1.88 | -10.80 | -0.22 | 2077.61 | 1804.31 | -273.30 | -5.69 | -4.81 |
| W | 32 | 53.37 | 49.86 | -3.51 | -6.58 | -0.14 | 2110.52 | 1911.47 | -199.05 | -4.15 | -3.85 |
| NW | 53 | 108.31 | 102.63 | -5.68 | -5.24 | -0.11 | 2206.17 | 1972.76 | -233.41 | -4.86 | -4.43 |
| Debris category (%) | | | | | | | | | | | |
| Debris-free | 90 | 53.61 | 45.27 | -8.34 | -15.56 | -0.32 | 1099.49 | 935.01 | -164.48 | -3.36 | -3.28 |
| 1-10 | 31 | 99.44 | 92.88 | -6.56 | -6.60 | -0.14 | 2920.20 | 2608.30 | -311.90 | -6.37 | -5.78 |
| 10--20 | 29 | 107.63 | 102.23 | -5.403 | -5.02 | -0.10 | 3195.20 | 2780.35 | -414.85 | -8.47 | -7.21 |
| 20--30 | 31 | 30.31 | 26.96 | -3.35 | -11.05 | -0.23 | 1830.87 | 1603.1 | -227.77 | -4.65 | -4.13 |
| 30--40 | 16 | 21.84 | 20.26 | -1.58 | -7.23 | -0.15 | 2098.18 | 1909.23 | -188.95 | -3.86 | -3.25 |
| >40 | 36 | 50.01 | 46.47 | -3.54 | -7.08 | -0.15 | 2045.97 | 1814.45 | -231.52 | -4.72 | -4.34 |
| Hypsometric class | | | | | | | | | | | |
| Very top-heavy (HI<–1.5) | 29 | 18.78 | 16.58 | -2.27 | -11.71 | -0.24 | 1158.67 | 992.82 | -165.78 | -3.38 | -3.12 |
| Top-heavy (–1.5<HI<–1.2) | 27 | 58.127 | 55.39 | -2.74 | -4.72 | -0.10 | 2020.77 | 1804.22 | -216.55 | -4.42 | -4.23 |
| Equidimensional (–1.2<HI<1.2) | 83 | 127.471 | 117.23 | -10.23 | -8.04 | -0.16 | 1855.56 | 1619.8 | -235.76 | -4.81 | -4.48 |
| Bottom-heavy (1.2 < HI < 1.5) | 56 | 92.45 | 83.31 | -9.16 | -9.85 | -0.20 | 1958.97 | 1736.33 | -222.64 | -4.54 | -4.51 |
| Very bottom-heavy (HI > 1.5) | 38 | 66.07 | 60.94 | -5.15 | -7.86 | -0.16 | 2350.31 | 2096.27 | -254.04 | -5.18 | -4.98 |

**Appendix 16** Results of Mann-Kendall tests of temperature for the Bhaga basin for three different types of datasets.

| Months/seasons | APHRODITE (1961-2015) | | | NCEP/NCAR (1948-2018) | | | University of Delaware (1901-2017) | | |
|---|---|---|---|---|---|---|---|---|---|
| | Test Z | Signific. | Sen slope | Test Z | Signific. | Sen slope | Test Z | Signific. | Sen slope |
| Jan | 0.799 | | 0.006 | 1.524 | | 0.011 | -0.459 | | -0.001 |
| Feb | 2.004 | * | 0.023 | 1.995 | * | 0.018 | 1.333 | | 0.005 |
| Mar | 1.858 | | 0.026 | 0.695 | | 0.005 | 0.342 | | 0.001 |
| Apr | 2.091 | * | 0.019 | -1.023 | | -0.007 | 1.067 | | 0.004 |
| May | 2.715 | ** | 0.031 | -0.511 | | -0.004 | 0.071 | | 0 |
| Jun | 0.900 | | 0.007 | -1.752 | | -0.012 | -1.395 | | -0.003 |
| Jul | 4.472 | *** | 0.023 | 1.137 | | 0.008 | -0.669 | | 0 |
| Aug | 5.474 | *** | 0.027 | 1.608 | | 0.006 | -0.327 | | 0 |
| Sep | 4.007 | *** | 0.023 | 0.477 | | 0.004 | -0.118 | | 0 |
| Oct | 3.107 | ** | 0.020 | 0.685 | | 0.008 | -0.210 | | 0 |
| Nov | 4.022 | *** | 0.028 | 4.289 | *** | 0.043 | 1.208 | | 0.003 |
| Dec | 3.775 | *** | 0.019 | 4.447 | *** | 0.035 | 0.978 | | 0.003 |
| Mean | 5.358 | *** | 0.022 | 2.154 | * | 0.010 | 1.211 | | 0.002 |
| Mean summer (Apr-Sep) | 5.096 | *** | 0.023 | 0.045 | | 0.000 | 0.158 | | 0.000 |
| Mean winter (Oct-March) | 4.211 | *** | 0.021 | 3.435 | *** | 0.020 | 1.274 | | 0.002 |
| Winter (Dec-Feb) | 2.802 | ** | 0.016 | 3.658 | *** | 0.019 | 0.789 | | 0.002 |
| pre-melting (Mar-may) | 2.846 | ** | 0.026 | -0.099 | | -0.001 | 0.954 | | 0.003 |
| Summer (Jun-Aug) | 4.109 | *** | 0.020 | 0.422 | | 0.002 | -1.237 | | -0.002 |
| Post-melting (Sep-Nov) | 5.372 | *** | 0.022 | 2.149 | * | 0.018 | 0.700 | | 0.001 |

**Note:** Significance level: * $P \leq 0.05$; ** $P \leq 0.01$; *** $P \leq 0.001$

**Appendix 17** Results of Mann-Kendall tests of precipitation for the Bhaga basin.

| Months/Seasons | APHRODITE (1951-2007) | | | NCEP/NCAR (1948-2008) | | | University of Delaware (1900-2017) | | |
|---|---|---|---|---|---|---|---|---|---|
| | Test Z | Signific. | Sen slope | Test Z | Signific. | Sen slope | Test Z | Signific. | Sen slope |
| Jan | -3.586 | *** | -1.010 | -2.194 | * | -0.065 | 0.561 | | 0.074 |
| Feb | -1.879 | + | -0.634 | 0.258 | | 0.013 | 1.561 | | 0.205 |
| Mar | -3.229 | ** | -1.232 | -2.124 | * | -0.065 | 1.412 | | 0.214 |
| Apr | -3.297 | *** | -0.852 | -0.824 | | -0.031 | 1.772 | + | 0.194 |
| May | -3.270 | ** | -0.809 | -2.938 | ** | -0.169 | 0.702 | | 0.074 |
| Jun | 0.406 | | 0.073 | -2.144 | * | -0.179 | 1.844 | + | 0.163 |
| Jul | -1.026 | | -0.323 | -1.549 | | -0.173 | -0.547 | | -0.050 |
| Aug | 1.081 | | 0.293 | -1.603 | | -0.128 | -1.407 | | -0.171 |
| Sep | -0.255 | | -0.074 | -1.181 | | -0.111 | 1.735 | + | 0.260 |
| Oct | -2.327 | * | -0.237 | -2.184 | * | -0.106 | 1.740 | + | 0.148 |
| Nov | -1.687 | + | -0.117 | 0.477 | | 0.021 | 3.203 | ** | 0.087 |
| Dec | -2.230 | * | -0.331 | -1.201 | | -0.033 | 1.312 | | 0.107 |
| Mean | -4.812 | *** | -0.511 | -2.943 | ** | -0.092 | 1.030 | | 0.038 |
| Mean summer (Apr-Sep) | -2.430 | * | -0.349 | -2.844 | ** | -0.141 | 0.053 | | 0.003 |
| Mean winter (Oct-March) | -4.757 | *** | -0.743 | -2.437 | * | -0.058 | 2.261 | * | 0.105 |
| Winter (Dec-Feb) | -4.454 | *** | -0.729 | -2.556 | * | -0.043 | 1.314 | | 0.084 |
| pre-melting (Mar-may) | -4.660 | *** | -1.023 | -2.665 | ** | -0.087 | 1.170 | | 0.098 |
| Summer (Jun-Aug) | 0.158 | | 0.031 | -2.199 | * | -0.171 | -1.102 | | -0.092 |
| Post-melting (Sep-Nov) | -1.645 | + | -0.246 | -1.171 | | -0.056 | 1.796 | + | 0.127 |

**Note:** Significance level: * $P \leq 0.05$; ** $P \leq 0.01$; *** $P \leq 0.001$

**Appendix 18** Glacier surface area change rate across the Himalaya.

| Region/ Basin/ Sub-basin | Glaciers | Period | Change (%) | Change rate (% $yr^{-1}$) | Data used | References |
|---|---|---|---|---|---|---|
| Western Himalaya | | | | | | |
| Ravi basin | | 1971–2010/2013 | 4.6 ± 4.1 | 0.1 ± 0.1 | Corona, Landsat, Worldview, Aster | Chand and Sharma 2015 |
| Saraswati/Alaknanda | | 1968–2006 | 4.6 ± 2.8 | 0.12 ± 0.07 | Corona, Landsat, ASTER, LISS IV, Cartosat | Bhambri et al. 2011 |
| Bhagirathi | | 1968–2006 | 5.7 ± 2.7 | 0.15 ± 0.7 | | |
| Nanga Parbat massif | | 1934-2019 | 7 | 0.1 | Topographical maps (1934), Corona, Hexagon, Landsat, Sentinel-2 | Nüsser and Schmidt 2021 |
| Kang Yatze Massif, Ladakh | | 1969–2010 | 14.3 | 0.3 | Corona, Landsat, Spot, Worldview | Schmidt and Nüsser 2012 |
| Central Ladakh Range | Phutse | 1969–2016 | 6.3 | 0.4 | Corona, Landsat, and field campaigns | Schmidt and Nüsser 2017 |
| | Nangtse | | 7.2 | 0.5 | | |
| Stok Range | | | 22.4 | 0.5 | | |
| Kang Yatze Range | | | 21.4 | 0.5 | | |
| Lungser Range | | | 17.7 | 0.4 | | |
| Ladakh range | | 1991–2014 | 12.8 | 0.6 | Landsat TM, ETM+, OLI | Chudley et al. 2017 |
| Chenab basin | | 1962–2001/2004 | 21.3 | 0.5 | SOI Maps, LISS III | Kulkarni et al. 2007 |
| Parbati basin | | | 22.4 | 0.52 | | |
| Baspa basin | | | 19.1 | 0.45 | | |
| Goriganga basin | | 1962–2001/2004 | 19.3 | 0.45 | SOI Maps, LISS III | Kulkarni et al. 2011 |
| Bhagirathi basin | | | 14.4 | 0.33 | | |
| Chandra basin | | | 20.1 | 0.48 | | |
| Bhaga basin | | | 30.2 | 0.71 | | |
| Miyar basin | | | 8.4 | 0.19 | | |
| Bhut basin | | | 10.3 | 0.24 | | |
| Warwan basin | | | 21.4 | 0.5 | | |
| Zanskar basin | | | 9.4 | 0.21 | | |
| Bhaga basin | Baralacha La | 1971–2011 | 16.37 ± 3.74 | 0.41 ± 0.09 | Corona, Landsat, LISS IV, Cartosat 1 | Negi et al. 2013 |
| Zanskar range | Parkachik | 1971–2015 | 1.5 ± 0.09 | 0.03± 0.002 | Corona, Landsat, GE | Mir and Majeed 2016 |
| Zansar range | Pensilungpa | 1977–2013 | 14.47 | 0.40 | Landsat | Shukla and Qadir 2016 |
| | Durung-drung | | 12.67 | 0.35 | | |
| | Haskira | | 20.74 | 0.58 | | |
| | Kange | | 13.61 | 0.38 | | |
| | Hagshu | | 15.55 | 0.43 | | |
| Chandrabhaga basin | | 1980–2010 | 2.5 | 0.08 | Landsat, LISS III, AWiFS | Pandey and Venkataraman 2013 |
| Alaknanda basin | Tipra | 1962–2008 | ~18 | 0.39 | SOI Maps, LISS III, Field observation | Mehta et al. 2011 |
| Kashmir Himalaya | Kolahai | 1962–2014 | 22.99 ± 2.3 | 0.44 ± 0.04 | SoI Maps, Landsat, Aster, LISS IV | Shukla et al. 2017 |
| Upper Tons basin | | 1962–2010 | 5.4 | 0.11 | SOI Maps, Landsat, LISS III, Field observation | Mehta et al. 2012 |
| Chandra basin | Samudra Tapu | 1962–2000 | 10.96 | 0.30 | SoI Maps, IRS PAN and LISS III | Kulkarni et al. 2006 |
| Kashmir Himalaya | | 1980–2013 | 17.92 | 0.54 | Landsat and Aster GDEM | Murtaza and Romshoo 2016 |
| Upper Chandra basin | Sakchum | 1993–2014 | 3.7 | 0.18 | Landsat, Terra ASTER, SRTM, Worldview | Garg et al. 2017 |
| | Chhota Shigri | | 1.26 | 0.06 | | |
| | Bara Shigri | | 0.92 | 0.04 | | |
| Chenab basin (Warwan-Bhut region) | | 1962–2001/02 | 11 | 0.28 | SoI maps, LISS III, AWiFS | Brahmbhatt et al. 2017 |
| Miyar basin | | 1989–2014 | 9 ± 0.7 | 0.36 ± 0.01 | Landsat and Aster GDEM | Patel et al. 2018 |

(-To be continued-)

**Appendix 18** Glacier surface area change rate across the Himalaya.(-Continued-)

| Region/ Basin/ Sub-basin | Glaciers | Period | Change (%) | Change rate (% $yr^{-1}$) | Data used | References |
|---|---|---|---|---|---|---|
| Bhaga basin | | 1971–2018 | 7.48 ± 2.17 | 0.17 ± 0.05 | Corona, Landsat, Sentinel 2A, ASTER GDEM v2 | Present Study |
| Central Himalaya | | | | | | |
| Kumbhu Himalaya | | 1962–2005 | 5.2 | 0.12 | Corona KH- 4, Landsat, Aster | Bolch et al. 2008 |
| Sagarmanthan National Park | | 1950–1990 | 4.9 | 0.12 | Based on topographic maps | Salerno et al. 2008 |
| Mt. Everest region | | 1974–2008 | 10.4 | 0.3 | Landsat MSS/TM, ASTER, ALOS/AVNIR2 | Ye et al. 2009 |
| Kanchenjunga–Sikkim area | | 1962–2000 | 19 ± 7 | 0.5 ± 0.2 | Corona KH- 4, Landsat, ASTER, Quick bird, Worldview | Racoviteanu et al. 2015 |
| Imja valley, Nepal | Nuptse | 1980–2010 | 27.3 | 0.91 | Landsat | Bajracharya et al. 2015 |
| | West Lhotse | | 54.9 | 1.83 | | |
| | Lhotse | | 30.6 | 1.02 | | |
| | Imja | | 16.2 | 0.54 | | |
| | East Amadablam | | 17.4 | 0.58 | | |
| | Amadablam | | 13 | 0.43 | | |
| | Duwo | | 5.3 | 0.18 | | |
| Eastern Himalaya | | | | | | |
| Sikkim Himalaya | | 1989/90–2010 | 3.3 ± 0.8 | 0.2 ± 0.1 | Landsat, LISS III | Basnett et al. 2013 |
| Bhutan Himalaya | | 1980–2010 | 23.3 ± 0.9 | 0.8 ± 0.03 | Landsat | Bajracharya et al. 2014 |
| Lunana area, Bhutan | Bechung | 1980–2010 | 18.6 | 0.62 | Landsat | Bajracharya et al. 2015 |
| | Raphstreng | | 29.3 | 0.98 | | |
| | Thorthormi | | 14.5 | 0.48 | | |
| | Lugge | | 21.2 | 0.71 | | |
| | Drukchang | | 8.2 | 0.27 | | |

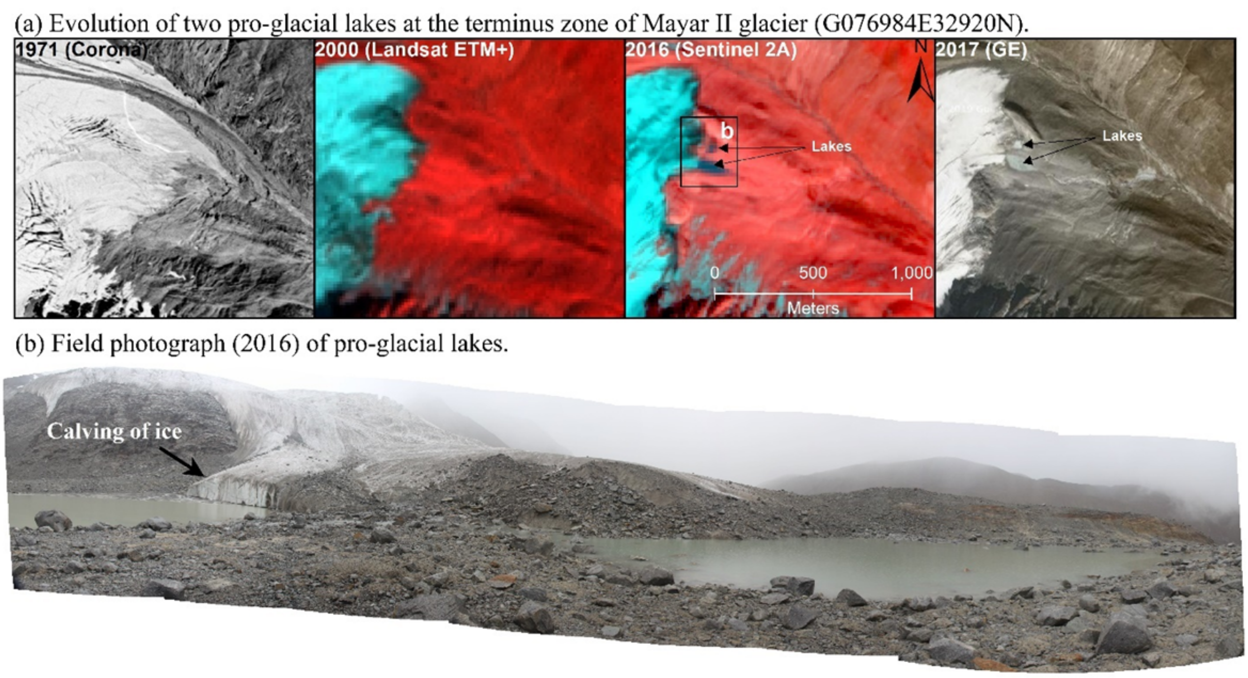


**Appendix 19** (a) Evolution of proglacial lakes at the terminus zone of the Mayar II Glacier in the Jankar Chhu watershed, Bhaga basin during 1971 and 2017. (b) Field photographs of lakes. Calving of ice is visible in one lake.

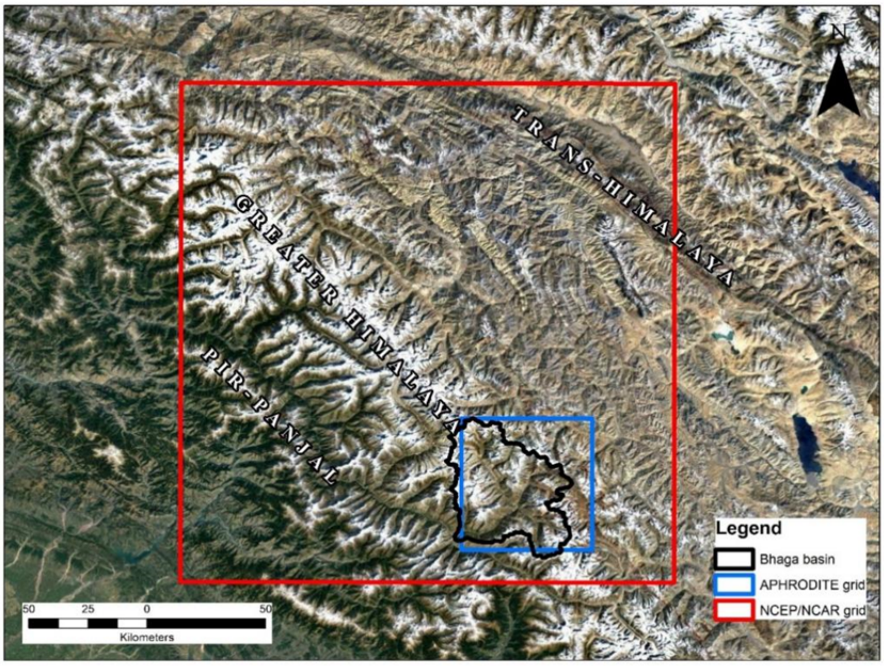


**Appendix 20** Spatial extent of single NCEP/NCAR and APHRODITE grid. One NCEP/NCAR grid extent is 2.5° (~277 km² at ground resolution). On the other hand, the APHRODITE grid extent is 0.5° (~55 km² at ground resolution). In this study, the analyzed NCEP/NCAR grid (32.5°N and 77.5°E) covers a vast area spanning from monsoon-dominated Pir-Panjal to the arid trans-Himalayan range. In contrast, APHRODITE represents a smaller area with the same microclimatic region.

## Additional references


Andreassen LM, Paul F, Kaab A, Hausberg JE (2008) Landsat-derived glacier inventory for Jotunheimen, Norway, and deduced glacier changes since the 1930s. Cryosphere 2:131–145. https://doi.org/10.5194/tc-2-131-2008

Bajracharya SR, Maharjan SB, Shrestha F, et al. (2015) The glaciers of the Hindu Kush Himalayas: current status and observed changes from the 1980s to 2010. Int J Water Resour Dev 31:161–173. https://doi.org/10.1080/07900627.2015.1005731

Bajracharya SR, Maharjan SB, Shrestha F (2014) Understanding dynamics of Himalayan glaciers: scope and challenges of remote sensing. Int Arch Photogramm Remote Sens Spat Inf Sci XL–8:1283–1289. https://doi.org/10.5194/isprsarchives-XL-8-1283-2014

Basnett S, Kulkarni A V., Bolch T (2013) The influence of debris cover and glacial lakes on the recession of glaciers in Sikkim Himalaya, India. J Glaciol 59:1035–1046. https://doi.org/10.3189/2013JoG12J184

Bhambri R, Bolch T, Chaujar RK (2012) Frontal recession of Gangotri Glacier, Garhwal Himalayas, from 1965 to 2006, measured through high- resolution remote sensing data. Curr Sci 102:1462–1466. https://www.zora.uzh.ch/id/eprint/59630/

Bhambri R, Bolch T, Chaujar RK, Kulshreshtha SC (2011) Glacier changes in the Garhwal Himalaya, India, from 1968 to 2006 based on remote sensing. J Glaciol 57:543–556. https://doi.org/10.3189/002214311796905604

Bolch T, Buchroithner M, Pieczonka T, Kunert A (2008) Planimetric and volumetric glacier changes in the Khumbu Himal, Nepal, since 1962 using Corona, Landsat TM and ASTER data. J Glaciol 54:592–600. https://doi.org/10.3189/002214308786570782

Bolch T, Menounos B, Wheate R (2010) Landsat-based inventory of glaciers in western Canada, 1985-2005. Remote Sens Environ 114:127–137. https://doi.org/10.1016/j.rse.2009.08.015

Brahmbhatt RM, Bahuguna IM, Rathore BP, et al. (2017) Significance of glacio-morphological factors in glacier retreat: a case study of part of Chenab basin, Himalaya. J Mt Sci 14:128–141. https://doi.org/10.1007/s11629-015-3548-0

Chand P, Sharma MC (2015) Glacier changes in the Ravi basin, North-Western Himalaya (India) during the last four decades (1971-2010/13). Glob Planet Change 135:133–147. https://doi.org/10.1016/j.gloplacha.2015.10.013

Chudley TR, Miles ES, Willis IC (2017) Glacier characteristics and retreat between 1991 and 2014 in the Ladakh range, Jammu and Kashmir. Remote Sens Lett 8:518–527. https://doi.org/10.1080/2150704X.2017.1295480

Garg PK, Shukla A, Tiwari RK, Jasrotia AS (2017) Assessing the status of glaciers in part of the Chandra basin, Himachal HimalayaA multiparametric approach. Geomorphology 284:99–114. https://doi.org/10.1016/j.geomorph.2016.10.022

Kulkarni A V, Bahuguna IM, Rathore BP, et al. (2007) Glacial retreat in Himalaya using Indian Remote Sensing satellite data. Curr Sci 92:69–74.

Kulkarni A V, Dhar S, Rathore BP, et al. (2006) Recession of Samudra Tapu glacier, Chandra river basin , Himachal Pradesh. J Indian Soc Remote Sens 34:39-46. https://doi.org/10.1007/BF02990745

Kulkarni A V, Rathore BP, Singh SK, Bahuguna IM (2011) Understanding changes in the Himalayan cryosphere using remote sensing techniques. Int J Remote Sens 32:601–615. https://doi.org/10.1080/01431161.2010.517802
Mehta M, Dobhal DP, Bisht MPS (2011) Change of Tipra glacier in the Garhwal Himalaya, India, between 1962 and 2008. Prog Phys Geogr 35:721–738. https://doi.org/10.1177/0309133311411760
Mehta M, Dobhal DP, Pratap B, et al. (2012) Glacier changes in Upper Tons River basin, Garhwal Himalaya, Uttarakhand, India. Zeitschrift fur G 57:225–244. https://doi.org/10.1127/0372-8854/2012/0095
Mir RA, Majeed Z (2016) Frontal recession of Parkachik Glacier between 1971-2015, Zanskar Himalaya using remote sensing and field data. Geocarto Int 6049:1–15. https://doi.org/10.1080/10106049.2016.1232439
Murtaza KO, Romshoo SA (2016) Recent glacier changes in the Kashmir Alpine Himalayas, India. Geocarto Int 6049:1–18. https://doi.org/10.1080/10106049.2015.1132482
Negi HS, Saravana G, Rout R, Snehmani (2013) Monitoring of great Himalayan glaciers in Patsio region, India using remote sensing and climatic observations. Curr Sci 105:1383–1392.
Patel LK, Sharma P, Fathima TN, Thamban M (2018) Geospatial observations of topographical control over the glacier retreat, Miyar basin, Western Himalaya, India. Environ Earth Sci 77:1–12. https://doi.org/10.1007/s12665-018-7379-5
Paul F, Kääb A, Maish M, et al. (2002) The new remote sensing derived Swiss glacier inventory: I Methods. Ann Glaciol 34:362–366. https://doi.org/10.3189/172756402781817941
Paul F, Winsvold SH, Kääb A, et al. (2016) Glacier Remote Sensing Using Sentinel-2. Part II: Mapping Glacier Extents and Surface Facies, and Comparison to Landsat 8. Remote Sens 8:1–15. https://doi.org/10.3390/rs8070575
Racoviteanu AE, Arnaud Y, Williams MW, Manley WF (2015) Spatial patterns in glacier characteristics and area changes from 1962 to 2006 in the Kanchenjunga-Sikkim area, eastern Himalaya. Cryosphere 9:505–523. https://doi.org/10.5194/tc-9-505-2015
Racoviteanu AE, Arnaud Y, Williams MW, Ordonez J (2008) Decadal changes in glacier parameters in the Cordillera Blanca, Peru, derived from remote sensing. J Glaciol 54:499–510. https://doi.org/10.3189/002214308785836922
Racoviteanu AE, Paul F, Raup B, et al. (2009) Challenges and recommendations in mapping of glacier parameters from space: results of the 2008 Global Land Ice Measurements from Space (GLIMS) workshop, Boulder, Colorado, USA. Ann Glaciol 50:53–69. https://doi.org/10.3189/172756410790595804
Rastner P, Bolch T, Mölg N, et al. (2012) The first complete inventory of the local glaciers and ice caps on Greenland. Cryosphere 6:1483–1495. https://doi.org/10.5194/tc-6-1483-2012
Salerno F, Buraschi E, Bruccoleri G, et al. (2008) Glacier surface-area changes in Sagarmatha national park, Nepal, in the second half of the 20th century, by comparison of historical maps. J Glaciol 54:738–752. https://doi.org/10.3189/002214308786570926
Schmidt S, Nüsser M (2012) Changes of High-Altitude Glaciers from 1969 to 2010 in the Trans-Himalayan Kang Yatze Massif, Ladakh, Northwest India. Arct Antract Alp Res 44:107–121. https://doi.org/10.1657/1938-4246-44.1.107
Shukla A, Ali I, Hasan N, Romshoo SA (2017) Dimensional changes in the Kolahoi glacier from 1857 to 2014. Environ Monit Assess 189:1–18. https://doi.org/10.1007/s10661-016-5703-7
Silverio W, Jaquet J-M (2005) Glacial cover mapping (1987 – 1996) of the Cordillera Blanca (Peru) using satellite imagery. Remote Sens Environ 95:342–350. https://doi.org/10.1016/j.rse.2004.12.012
Wang L, Li Z, Wang F, et al. (2014) Glacier changes from 1964 to 2004 in the Jinghe River basin, Tien Shan. Cold Reg Sci Technol 102:78–83. https://doi.org/10.1016/j.coldregions.2014.02.006
Ye Q, Zhong Z, Kang S, et al. (2009) Monitoring glacier and supra-glacier lakes from space in Mt. Qomolangma region of the Himalayas on the Tibetan Plateau in China. J Mt Sci 6:211–220. https://doi.org/10.1007/s11629-009-1016-4